Cutting in-line with iron: ribosomal function and non-oxidative RNA cleavage

Rebecca Guth-Metzler[1,2†], Marcus S. Bray[2,3†§], Suttipong Suttapitugsakul[1], Claudia Montllor-Albalate[1], Jessica C. Bowman[1,2], Ronghu Wu[1], Amit R. Reddi[1], C. Denise Okafor[4], Jennifer B. Glass[2,5*], and Loren Dean Williams[1,2*]

[1]School of Chemistry and Biochemistry, Georgia Institute of Technology, Atlanta, GA, USA, 30332
[2]NASA Center for Origins of Life, Georgia Institute of Technology, Atlanta, GA, USA, 30332
[3]School of Biological Sciences, Georgia Institute of Technology, Atlanta, GA, USA, 30332
[4]Department of Biochemistry and Molecular Biology, The Pennsylvania State University, University Park, PA, 16802
[5]School of Earth and Atmospheric Sciences, Georgia Institute of Technology, Atlanta, GA, USA, 30332

*To whom correspondence should be addressed: Tel: (404) 385-6258; Fax: (404) 894-2295; Email: Loren.Williams@chemistry.gatech.edu; Email: Jennifer.Glass@eas.gatech.edu;

[†]These authors contributed equally to this work.

[§]Present Address: Department of Biology, San Diego State University, San Diego, CA, 92182

Abstract

Divalent metal cations are essential to the structure and function of the ribosome. Previous characterizations of ribosome structure and function performed under standard laboratory conditions have implicated Mg^{2+} as the primary mediator of ribosomal structure and function. The contribution of Fe^{2+} as a ribosomal cofactor has been largely overlooked, despite the ribosome's evolution in a high Fe^{2+} environment, and its continued use by obligate anaerobes inhabiting high Fe^{2+} niches. Here we show that (i) iron readily cleaves RNA by a non-oxidative mechanism that has not been detected previously, (ii) functional ribosomes purified from cells grown under low O_2, high Fe^{2+} conditions are associated with Fe^{2+}, (iii) a small subset of Fe^{2+} that is associated with the ribosome is not exchangeable with surrounding cations, presumably because they are highly coordinated by rRNA. In total, these results expand the ancient role of iron in biochemistry, suggest a novel method for regulation of translation by iron, and highlight a possible new mechanism of iron toxicity.

Key Points:

1) iron readily cleaves RNA by a non-oxidative mechanism that has not been detected previously;
2) functional ribosomes purified from cells grown under low O_2, high Fe^{2+} conditions are associated with Fe^{2+};
3) a small subset Fe^{2+} that is associated with the ribosome is not exchangeable.

Introduction

The ribosome is responsible for the synthesis of all coded proteins and contains life's most conserved ribonucleic acids. The common core of the ribosome is universal to all life (1,2) and has been essentially invariant since the last universal common ancestor (3-5). Thus, ribosomes can be interrogated as molecular fossils (6-8). Because ribosomal structure and function are strongly dependent on divalent cations (M^{2+}) (9), and because ribosomes originated long before the Great Oxidation Event (GOE), understanding ribosomal origins and evolution requires characterization of ribosomal interactions with M^{2+} ions under pre-GOE conditions (10-14).

In extant aerobic life, Mg^{2+} appears to be the dominant M^{2+} ion in the translation system. Hundreds of Mg^{2+} ions mediate ribosomal RNA (rRNA) folding and ribosomal assembly, in some instances binding to specific sites in the universal rRNA common core by direct coordination (9,15-17). Mg^{2+} ions facilitate association of the large ribosomal subunit (LSU) and small ribosomal subunit (SSU) (18), stabilize folded tRNA (19), maintain the reading frame during translation (20), and link ribosomal proteins (rProteins) to rRNA (21).

Before the GOE, anoxia would have stabilized abundant Fe^{2+} in the biosphere and hydrosphere. Under pre-GOE conditions, Fe^{2+} would not have caused the oxidative damage to biomolecules that occurs today in the presence of O_2, via Fenton chemistry (22). We recently reported that Fe^{2+} can mediate *in vitro* translation under "pre-GOE" conditions: in the presence of abundant Fe^{2+} and in the absence of O_2 (23,24). Based on these findings, we proposed that early ribosomal folding and catalysis used Fe^{2+} instead of, or in combination with Mg^{2+} and other M^{2+} ions. However, our observation of lower translation rates with anoxic Fe^{2+} than with Mg^{2+} (23) suggests that Fe^{2+} might mediate non-oxidative damage of RNA at faster rates than Mg^{2+}.

Here we demonstrate that Fe^{2+} can damage RNA, and the ribosome, by two separate and distinct mechanisms. The first mechanism is the well-known Fenton reaction (22) whereby the reaction of Fe^{2+} with O_2 or H_2O_2 generates hydroxyl radicals, causing oxidative damage of nucleic acids (25-29). A second, non-oxidative mechanism of Fe^{2+}-mediated RNA damage can be more extensive in some conditions than oxidative damage. We have discovered that in-line cleavage of RNA is catalyzed by Fe^{2+} by promoting the attack of a ribose 2'-hydroxyl group on the proximal phosphorous. The catalysis of in-line cleavage by Mg^{2+} is well established (30,31). Mg^{2+}-mediated in-line cleavage has been used, for example, to detect changes in RNA conformation upon binding of target compounds to riboswitches (32,33). Other metals are known to cleave RNA by non-oxidative processes. Europium, lead, or terbium have been used to monitor RNA folding or to identify metal binding sites (34-37). Here we show that anoxic Fe^{2+} is efficient in catalyzing in-line cleavage, cleaving RNA far more rapidly and extensively than Mg^{2+}.

We have also investigated whether ribosomes in *E. coli* grown in pre-GOE conditions associate functionally with Fe^{2+} *in vivo*. We have grown *E. coli* in anoxic conditions with ample Fe^{2+} in the growth media. We have purified ribosomes from these bacteria and have probed their interactions with metals. We have identified tightly bound M^{2+}, which survive ribosomal purification. A small subset of Fe^{2+} ions are not exchangeable with Mg^{2+} in solution and are detectable after purification involving repeated washes in high [Mg^{2+}] buffers. We use these tightly bound ions as reporters for more general M^{2+} association *in vivo*. The data are consistent with a model in which certain M^{2+} ions are deeply buried and highly coordinated within the ribosome (16). Indeed, our results suggest that ribosomes grown in pre-GOE conditions contain

~10 tightly bound Fe^{2+} ions compared to ~1 Fe^{2+} ion in ribosomes from standard growth conditions. Ribosomes washed with Fe^{2+} contained significantly higher Fe^{2+} and showed more rRNA degradation than ribosomes washed with Mg^{2+}. Our combined results show the capacity for Fe^{2+} to (i) associate with functional ribosomes *in vivo* and *in vitro* and (ii) mediate significant non-oxidative damage.

Materials and Methods

Cell culture and harvesting. Culturing media consisted of LB broth (10 g L^{-1} NaCl, 10 g L^{-1} tryptone, 5 g L^{-1} yeast extract) amended with 4 mM tricine, 50 mM sodium fumarate, and 80 mM 3-(N-morpholino)propanesulfonic acid (MOPS; pH 7.8). Fifty mL cultures containing all of these ingredients plus 0.25% v/v glycerol were inoculated from glycerol stocks of *Escherichia coli* MRE600 cells and shaken overnight at 37□C with or without O_2 and with either 1 mM $FeCl_2$ or ambient Fe^{2+}[6-9 µM, measured by the ferrozine assay (38)]. Two mL of each overnight culture was used to inoculate 1-L cultures in the same conditions. These cultures were then orbitally shaken at 37□C to OD_{600} 0.6-0.7. Aerobic cultures were grown in foil-covered Erlenmeyer flasks. Anaerobic fumarate-respiring cultures were inoculated into stoppered glass bottles containing medium that had been degassed with N_2 for one hour to remove O_2. Cells were then harvested by centrifugation at 4,415 x g for 10 minutes, washed in 20 mL buffer containing 10 mM Tris pH 7.4, 30 mM NaCl, and 1 mM EDTA, and pelleted at 10,000 x g for 10 minutes. Cell pellets were stored at -80°C until ribosome purification.

Ribosome purification. The ribosome purification procedure was modified from Maguire et. al (39). All purification steps were performed in a Coy anoxic chamber (97% Ar, 3% H_2 headspace) unless otherwise noted. Buffers varied in their metal cation content. The typical wash buffer contained 100 mM NH_4Cl, 0.5 mM EDTA, 3 mM β-mercaptoethanol, 20 mM Tris pH 7.5, 3 mM $MgCl_2$, and 22 mM NaCl. For "Fe purification" experiments, buffer was composed of 100 mM NH_4Cl, 0.5 mM EDTA, 3 mM β-mercaptoethanol, 20 mM Tris pH 7.5, 1 mM $FeCl_2$ and 28 mM NaCl. Sodium chloride concentrations were increased here to maintain the ionic strength of the buffer (131 mM). Elution buffers contained the same composition as the wash buffer except for NH_4Cl (300 mM). Frozen cell pellets were resuspended in ribosome wash buffer and lysed in a BeadBug microtube compact homogenizer using 0.5 mm diameter zirconium beads (Benchmark Scientific). Cell lysate was transferred into centrifuge bottles inside the anoxic chamber which were tightly sealed to prevent O_2 contamination. Cell debris were removed by centrifuging outside of the anoxic chamber at 30,000 x g for 30 minutes at 4□C. The soluble lysate was then transferred back into the chamber and loaded onto a column containing pre-equilibrated, cysteine-linked, SulfoLink™ Coupling Resin (Thermo Fisher Scientific). The resin was washed with 10 column volumes of wash buffer. Ribosomes were eluted into three 10 mL fractions with elution buffer. Eluted fractions were pooled inside the anoxic chamber into ultracentrifuge bottles which were tightly sealed. Ribosomes were pelleted outside the chamber by centrifuging at 302,000 x g for 3 hours at 4□C under vacuum in a Beckman Optima XPN-100 Ultracentrifuge using a Type 70 Ti rotor. Tubes containing ribosome pellets were brought back into the chamber and suspended in buffer containing 20 mM N-(2-hydroxyethyl)piperazine-N'-2-ethanesulfonic acid (HEPES; pH 7.6), 30 mM KCl, and 7 mM β-mercaptoethanol, heat-sealed in mylar bags, and stored at -80□C. Ribosome concentrations were calculated with a NanoDrop spectrophotometer assuming $1A_{260}$ = 60 µg ribosome mL^{-1} (conversion factor provided by New England Biolabs). This conversion factor was used to estimate the molecular mass of bacterial

ribosomes, from which molarity was calculated. Biological triplicates of each growth/purification method were taken for downstream analyses.

Ribosomal Fe content. Purified ribosomes were analyzed for iron content by total reflection X-ray fluorescence spectroscopy (TRXF) as described in Bray and Lenz et al (23).

Ribosomal RNA purification. rRNA was isolated from purified ribosomes by phenol chloroform extraction and suspended in 0.1 mM EDTA. RNA concentrations were quantified by A_{260} ($1A_{260}$ = 40 µg rRNA mL^{-1}).

rProtein electrophoresis. For SDS-PAGE, purified ribosomes were normalized to 3.33 mg mL^{-1} in 2X SDS-PAGE dye, heated at 95□C for 5 minutes, and then incubated on ice for 2 minutes. Samples were loaded onto a 12% SDS acrylamide gel with a 4% stacking gel and run at 180 V for 60 minutes.

In vitro translation. Translation reactions were based on the methods of Bray and Lenz et al. (23) with minor modifications. All 15 µL reactions contained 2.25 µL of purified ribosome samples normalized to 9 µg $µL^{-1}$ (so that the final concentration of ribosomes in our reactions was 1.35 µg $µL^{-1}$), 0.1 mM amino acid mix, 0.2 mM tRNAs, ~0.2 µg $µL^{-1}$ of dihydrofolate reductase mRNA, and 3 µL of factor mix (with RNA polymerase, and transcription/translation factors in 10 mM Mg^{2+}) from the PURExpress® Δ Ribosome Kit (New England Biolabs). The reaction buffer was based on Shimizu et al. (40), with HEPES-OH instead of phosphate buffer to avoid precipitation of metal phosphates. Buffer consisted of 20 mM HEPES-OH (pH 7.3), 95 mM potassium glutamate, 5 mM NH_4Cl, 0.5 mM $CaCl_2$, 1 mM spermidine, 8 mM putrescine, 1 mM dithiothreitol (DTT), 2 mM adenosine triphosphate (ATP), 2 mM guanosine triphosphate (GTP), 1 mM uridine triphosphate (UTP), 1 mM cytidine triphosphate (CTP), 10 mM creatine phosphate (CP), and 53 µM 10-formyltetrahydrofolate. Divalent cation salts ($MgCl_2$ or $FeCl_2$) were added to 9 mM final concentration. The reaction buffer was lyophilized and stored at -80°C until resuspension in anoxic nuclease-free water immediately before experiments in the anoxic chamber. Reaction mixtures were assembled in the anoxic chamber and run at 37°C in a heat block for 120 minutes. Reactions were quenched on ice and stored on ice until they were assayed for the extent of protein synthesis. Protein synthesis was measured using a DHFR assay kit (Sigma-Aldrich), which measures the oxidation of NADPH (60 mM) to $NADP^+$ by dihydrofolic acid (51 µM). Assays were performed by adding 5 µL of protein synthesis reaction to 995 µL of 1X assay buffer. The NADPH absorbance peak at 340 nm (Abs_{340}) was measured in 15 s intervals over 2.5 minutes. The slope of the linear regression of Abs_{340} vs. time was used to estimate protein activity (Abs_{340} min^{-1}).

In-line cleavage reaction rates. Nuclease free water (IDT) was used in all experiments involving purified or transcribed RNA. rRNA for in-line cleavage experiments was purified by phenol-chloroform extraction followed by ethanol precipitation of commercial *E. coli* ribosomes (New England Biolabs, Ipswich MA, USA; catalog # P0763S). All in-line cleavage reaction solutions were prepared and incubated in the anoxic chamber Fe and Mg solutions were prepared by dissolving a known mass of $FeCl_2$-$4H_2O$ or $MgCl_2$ salt in degassed water inside the chamber. 0.5 µg $µL^{-1}$ of rRNA was suspended in degassed 20 mM HEPES pH 7.6, 30 mM KCl, 5% v/v glycerol [Invitrogen (UltraPure)], and either 25 mM of $MgCl_2$ or 1 mM of $FeCl_2$ both with and without 100 mM EDTA. Reactions were placed on a 37□C heat block and incubated for 4 days for the $MgCl_2$ and no M^{2+} conditions and for 8 hours for the $FeCl_2$ conditions. At each time point

(0, 1.5, 3, 6, 12, 24, 48, and 96 hours for the $MgCl_2$ and no M^{2+} conditions and 0, 7.5, 15, 30, 60, 120, 240, and 480 minutes for the $FeCl_2$ conditions) 4.5 µL aliquots were combined with 0.5 µL of 1 M sodium phosphate buffer pH 7.6 to precipitate the Fe^{2+} or Mg^{2+} from solution and stored at -80□C. Aliquots were defrosted on ice and combined with 2X Gel Loading Buffer II (Amicon) then loaded onto a 1% Tris/Borate/EDTA agarose gel and run at 120V for 1.25 hours. The gel was stained with GelStar™ and imaged with an Azure 6000 Imaging System (Azure Biosystems). Azurespot software was used as a pixel counter to create lane profiles. rRNA peaks were integrated by fitting to an Exponentially Modified Gaussian distribution using Igor Pro (v 7.08), which calculated discrepancies between fits and observed peaks. Observed rate constants (k_{obs}) were found by taking the negative of the slope from the natural logarithm of the normalized peak area vs. time plot. Uncertainties reported on the plots as error bars are discrepancies between fits and observed peaks. The uncertainties of k_{obs} values were estimated with the LINEST function in Excel. Rate constants (k) were calculated by $k = k_{obs}/[M^{2+}]$. The uncertainties of k's were estimated using k_{obs}, the uncertainties of k_{obs}, $[M^{2+}]$ and the uncertainties of $[M^{2+}]$ through following the equation (41).

$$\sigma_k = \sqrt{\frac{(\sigma_{k_{obs}})^2}{[M^{2+}]^2} + \frac{(k_{obs})^2(\sigma_{[M^{2+}]})^2}{[M^{2+}]^4}} \quad \#\text{Equation 1}$$

Empirical error analysis confirms the assumption of equation 1 that systematic errors in [rRNA], caused for example by the approximate nature of the rRNA extinction coefficient, do not cause errors in k.

In-line cleavage banding patterns. a-rRNA (42), which is composed of the core of the LSU rRNA, was synthesized and purified as previously described. Lyophilized a-rRNA was resuspended in degassed nuclease free water (IDT) inside the anoxic chamber. Fe and Mg solutions were prepared by dissolving known amounts of $FeSO_4$-$7H_2O$ or $MgSO_4$ in degassed nuclease free water inside the anoxic chamber. To initiate the reaction, 1 mM (final concentration) of Mg or Fe was added to 0.02 µg μL^{-1} a-rRNA in 20 mM HEPES-TRIS (pH 7.2) in a 37°C heating block. Samples were removed at 0, 0.25, 0.5, and 1 hrs for added Fe^{2+} and 1 hr for added Mg^{2+}, and divalent chelation beads (Hampton Research) were added to quench the reactions. Chelation beads were removed using spin columns. The RNA cleavage products were visualized using denaturing PAGE (6%, 8M urea) run at 120 V for ~1.3 hours stained with SYBR Green II.

Fenton chemistry reactions. Purified rRNA from *E. coli* ribosomes (New England Biolabs) was obtained by phenol-chloroform extraction and ethanol precipitation. A stock solution of Fe/EDTA was prepared inside the anoxic chamber by dissolving a known amount of $FeCl_2$-$4H_2O$ salt in degassed water then mixing with EDTA in degassed water. The Fe/EDTA was removed from the chamber for the Fenton reactions. Ribosomal RNA was suspended to 0.5 µg μL^{-1} in 20 mM HEPES pH 7.6, and 30 mM KCl, with 0% or 5% v/v glycerol and either 1 mM Fe/10 mM EDTA/10 mM ascorbate plus 0.3% v/v H_2O_2 or 10 mM EDTA as the reaction initiators wherein the initiators were separately dispensed onto the tube wall and vortexed with the other components. For the zero time points, reaction components were mixed in tubes containing the thiourea quenching agent at a final concentration of 100 mM. For non-zero time points the reaction mixtures were prepared as bulk solutions and incubated at 37□C on a heat block, after which aliquots were removed at 0, 10, and 60 minutes and mixed with the thiourea quenching agent at a final concentration of 100 mM. The stopped solutions were immediately frozen and

stored at -80□C. For analysis, samples were defrosted on ice, combined with 2X Gel Loading Buffer II (Amicon), loaded onto a 1% Tris/Borate/EDTA agarose gel and run at 120V for 1.25 hours.

Protein characterization by LC-MS/MS. Protein solutions were reduced with β-mercaptoethanol, and then alkylated with 14 mM iodoacetamide for 30 minutes at room temperature in the dark. Alkylation was quenched with 5 mM dithiothreitol for 15 minutes at room temperature in the dark. Proteins were purified by the methanol/chloroform purification method and digested with trypsin in a buffer containing 5% acetonitrile, 1.6 M urea, and 50 mM HEPES pH 8.8 at 37^{o}C with shaking overnight. The digestion was quenched with 1% formic acid. Peptides were purified by Stage-Tip (43) prior to LC-MS/MS analysis.

Peptides were dissolved in 5% acetonitrile and 4% formic acid and loaded onto a C18-packed microcapillary column (Magic C18AQ, 3 μm, 200 Å, 75 μm x 16 cm, Michrom Bioresources) by a Dionex WPS-3000TPL RS autosampler (Thermostatted Pulled Loop Rapid Separation Nano/Capillary Autosampler). Peptides were separated by a Dionex UltiMate 3000 UHPLC system (Thermo Scientific) using a 112-minute gradient of 4-17% acetonitrile containing 0.125% formic acid. The LC was coupled to an LTQ Orbitrap Elite Hybrid Mass Spectrometer (Thermo Scientific) with Xcalibur software (version 3.0.63). MS analysis was performed with the data dependent Top15 method; for each cycle, a full MS scan with 60,000 resolution and $1*10^6$ AGC (automatic gain control) target in the Orbitrap cell was followed by up to 15 MS/MS scans in the Orbitrap cell for the most intense ions. Selected ions were excluded from further sequencing for 90 seconds. Ions with single or unassigned charge were not sequenced. Maximum ion accumulation time was 1,000 ms for each full MS scan, and 50 ms for each MS/MS scan.

Raw MS files were analyzed by MaxQuant (version 1.6.2.3; 44). MS spectra were searched against the *E. coli* database from UniProt containing common contaminants using the integrated Andromeda search engine (45). Due to the unavailability of the proteome database for *E. coli* strain MRE-600, the database for strain K12 was used. It has been shown that the two strains have nearly identical ribosome associated proteins (46). All samples were searched separately and set as individual experiments. Default parameters in MaxQuant were used, except the maximum number of missed cleavages was set at 3. Label-free quantification was enabled with the LFQ minimum ratio count of 1. The match-between-runs option was enabled. The false discovery rates (FDR) were kept at 0.01 at the peptide and protein levels.

The results were processed using Perseus software (47). In the final dataset, the reverse hits and contaminants were removed. The LFQ intensity of each protein from the proteinGroups table was extracted and reported. For the volcano plots showing differential regulation of proteins, ratios used were from the LFQ intensities of samples from each of the three experiments. The cutoff for differential expression was set at 2-fold. P-values were calculated using a two-sided T-test on biological triplicate measurements with the threshold p-value of 0.05 for significant regulation. The raw files are publicly available at http://www.peptideatlas.org/PASS/PASS01418 (username: PASS01418 and password: ZW2939nnw).

Results

In-line cleavage of rRNA: Mg^{2+} and anoxic Fe^{2+}. By manipulating reaction conditions, we could switch the mode of rRNA cleavage between Fenton and in-line mechanisms. In-line is the only

possible mechanism of cleavage by Mg^{2+} due to its fixed oxidation state and inability to generate hydroxyl radicals. We confirm the expectation that Mg^{2+}-mediated in-line cleavage reactions are not inhibited by anoxia or hydroxyl radical quenchers. Mg^{2+}-mediated in-line cleavage reactions are inhibited by chelators, as expected for a mechanism that requires direct metal-RNA interaction.

We confirm here in a variety of experiments that RNA is degraded by in-line cleavage when incubated with Fe^{2+} under anoxic conditions (**Fig. 1a**). Most of the experiments employed the 16S rRNA of *E. coli* as substrate. A shorter RNA [a-RNA (42)] showed on a higher size resolution gel that RNA banding patterns and reaction products were nearly identical for Mg^{2+} and anoxic Fe^{2+} reactions (**Fig. 2**), indicating that preferred sites of cleavage are the same for both metals. Common sites of cleavage are indications of common mechanisms of cleavage (31). In the absence of O_2, cleavage by either Mg^{2+} or Fe^{2+} was inhibited by EDTA (**Fig. 1b,d**) as expected for a mechanism that requires direct metal-RNA interaction but not for a mechanism with a diffusible intermediate. Neither Mg^{2+} nor anoxic Fe^{2+} cleavage was inhibited by glycerol (5%), which is known to quench hydroxyl radical and to inhibit hydroxyl radical cleavage (48). By contrast, glycerol inhibited cleavage by Fe^{2+} under conditions that favor Fenton type cleavage. Glycerol did not inhibit Mg^{2+} in-line cleavage under any conditions **(Fe^{2+}: Fig. S1; Mg^{2+}: Fig. S2)**.

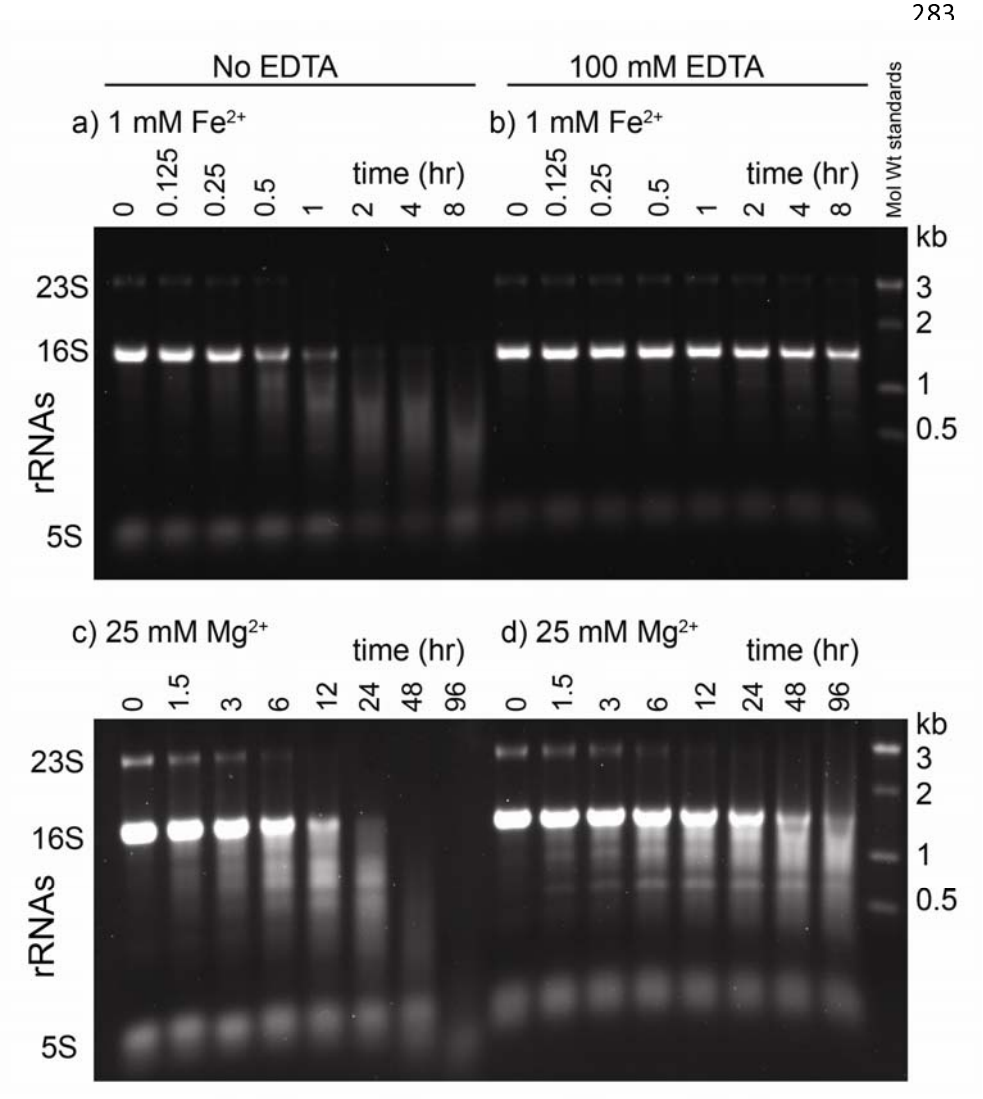

Figure 1. In-line cleavage of rRNA in anoxia. In-line cleavage of purified rRNAs with a) 1 mM Fe^{2+} (0-8 hr), b) 1 mM Fe^{2+} plus 100 mM EDTA (0-8 hr), c) 25 mM Mg^{2+} (0-96 hr), and d) 25 mM Mg^{2+} plus 100 mM EDTA (0-96 hr).. Reactions were conducted in an anoxic chamber at 37□C in the presence of the hydroxyl radical quencher glycerol (5% v/v) and were analyzed by 1% agarose gels.

In the absence of O_2, cleavage rates

are significantly greater for Fe^{2+} than for Mg^{2+}. For 16S and 23S rRNAs, 1 mM Fe^{2+} caused significant in-line cleavage of rRNA after 30 minutes at 37□C. Both rRNAs were completely degraded after 2 hours in anoxic Fe^{2+} (**Fig. 1a**). By contrast, when the M^{2+} ion was switched from 1 mM Fe^{2+} to 25 mM Mg^{2+}, only a modest amount of in-line cleavage was observed after 6 hours (**Fig. 1c**). Fitting of the data to a first order rate model **(Figure S3)** and converting k_{obs} to k using $k = k_{obs}[M^{2+}]$ reveals that the apparent rate constant for in-line cleavage of the full-length 16S rRNA is 0.45 ± 0.03 s^{-1} for Fe^{2+} and 0.00095 ± 0.00008 s^{-1} for Mg^{2+}. Addition of EDTA inhibited cleavage, with k dropping to 0.012 ± 0.002 s^{-1} for Fe^{2+} and 0.00016 ± 0.00003 s^{-1} for Mg^{2+}.

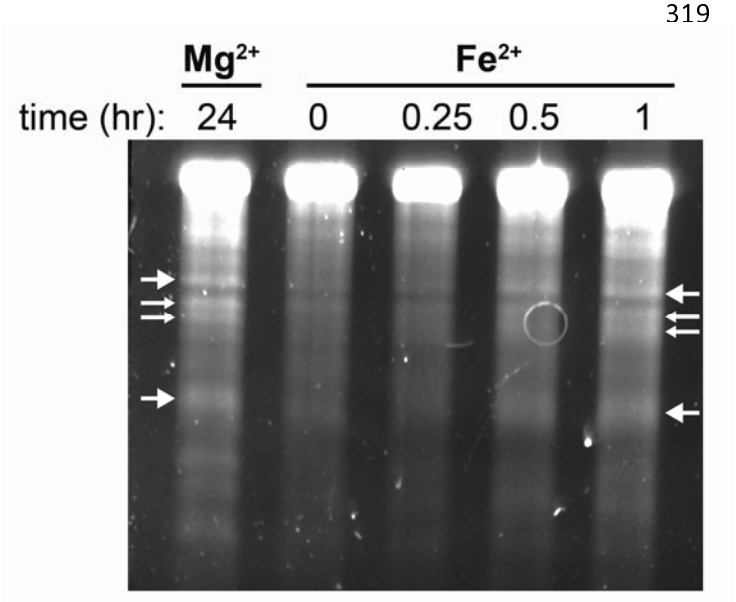

In sum, reactions with Mg^{2+} and anoxic Fe^{2+} and showed the same responses to potential inhibitors. Reactions with Fe^{2+} in the absence of O_2 were not inhibited by a hydroxyl radical quencher but were inhibited by a chelator. By contrast, reactions with Fe^{2+} in the presence of O_2 were inhibited by a hydroxyl radical quencher but not by a chelator. The apparent rate constant for inline cleavage is ~475-fold greater for Fe^{2+} than for Mg^{2+}.

Figure 2. In-line cleavage banding patterns are the same for rRNA cleavage with Mg^{2+} and anoxic Fe^{2+}. Several primary cleavage bands of a-rRNA (42) are indicated by arrows. This gel is 6% polyacrylamide, 8 M urea showing cleavage with in-line cleavage mediated by 1 mM Mg^{2+} or 1 mM anoxic Fe^{2+} at 37°C for varying amounts of time. Reactions were run in 20 mM Tris-HEPES, pH 7.2.

M^{2+} exchange during ribosomal purification. The vast majority of ribosomal M^{2+} ions are exchangeable. M^{2+} exchange takes place during purification. The Fe^{2+} content of purified ribosomes depended on the type of M^{2+} in the purification buffer. Ribosomes purified in solutions with 1 mM Fe^{2+} contained significantly higher Fe^{2+} than those purified in 3 mM Mg^{2+} (**Fig. 3**). All ribosome samples purified in 1 mM Fe^{2+} contained similar Fe^{2+} (~400-600 mol Fe mol^{-1} ribosome).

Tight ribosomal binding of a subset of M^{2+}. A small subset of ribosomal M^{2+} ions are not exchangeable during purification. Ribosomes retain this subset of *in vivo* divalent cations after purification. Ribosomes from *E. coli* grown in pre-GOE conditions (anoxic, high Fe^{2+}) contained quantitatively reproducible elevated levels of Fe^{2+} after purification in solutions containing Mg^{2+}. We detect around 9 mol Fe mol^{-1} ribosome from cells grown in pre-GOE conditions purified in solutions with high Mg^{2+} (**Fig. 3)**. Ribosome-associated Fe^{2+} was quantified with TXRF, as described previously (23). Three non-pre-GOE growth conditions yielded ribosomes containing near background levels of Fe^{2+} (< 2 mol Fe mol^{-1} ribosome). To make these comparisons, *E. coli* were harvested in log phase from each of four growth conditions: oxic or anoxic with high Fe^{2+}in

the medium (1 mM Fe^{2+}), and oxic or anoxic without added Fe^{2+} in the growth medium (6-9 µM Fe^{2+}).

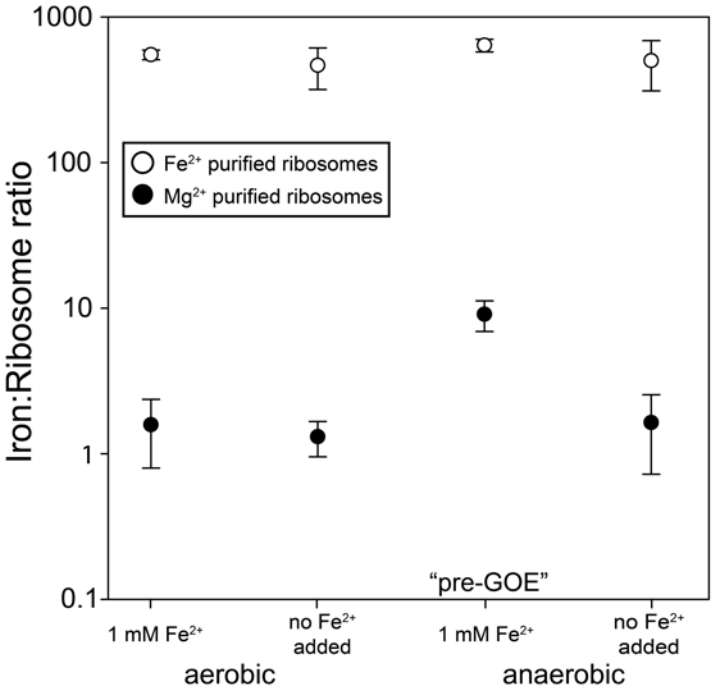

Figure 3. Iron content (mol Fe mol^{-1} ribosome) of purified ribosomes. *E. coli* were grown aerobically or anaerobically at 1 mM Fe^{2+} or ambient Fe^{2+} (6-9 µM, no Fe added), and purified in buffers containing either 3 mM Mg^{2+} (black circles) or 1 mM Fe^{2+} (white circles). Error bars represent standard error of the mean (n=3).

Quantitating translation. Ribosomes from all four growth conditions produced active protein in translation assays. Ribosomes were functional *in vitro* under standard conditions (with 10 mM Mg^{2+}) and also in 8 mM Fe^{2+} plus 2 mM Mg^{2+} under anoxia (**Table 1**). The rate of translation was slower in the presence of Fe^{2+} than in Mg^{2+}, consistent with our previous work (23). The translational activity of ribosomes harvested from anaerobic cells was slightly less than from those from aerobic cells. Ribosomes from all four growth conditions contained intact 23S, 16S, and 5S rRNAs with purification in 3 mM Mg^{2+} (**Fig. 4a**) resulting in a higher proportion of intact rRNA relative to purification in 1 mM Fe^{2+} (**Fig. 4b**). Each purification also contained a full suite of rProteins as indicated by mass spectrometric analysis and by gel electrophoresis (**Fig. S4**). The protein composition of ribosomes from 1 mM Fe^{2+} growth conditions (**Fig. S4b**) was similar to that from Mg^{2+} growth conditions (**Fig. S4a**).

Figure 4. 1% agarose gels showing rRNA from ribosomes purified in (a) 3 mM Mg^{2+} and (b) 1 mM Fe^{2+}. The banding pattern suggests that rRNA is relatively more intact in ribosomes purified with 3 mM Mg^{2+} than in ribosomes purified with 1 mM Fe^{2+}.

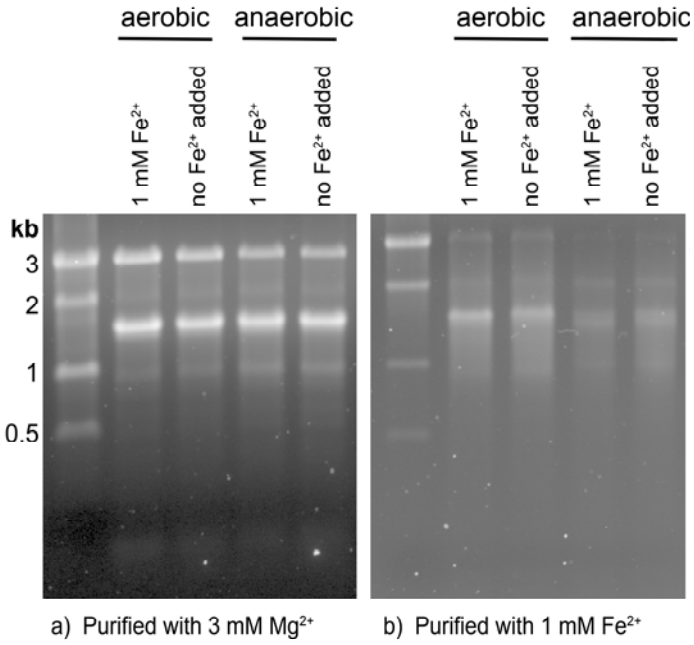

Table 1. *In vitro* translation activity of purified ribosomes[a].

Growth conditions		Translation activity (Abs_{340} min^{-1}) Translation reaction [M^{2+}]	
		10 mM Mg^{2+}	**8 mM Fe^{2+} + 2 mM Mg^{2+}**
Aerobic	1 mM Fe^{2+}	0.112 ± 0.005	0.027 ± 0.006
Aerobic	No Fe^{2+} added	0.100 ± 0.010	0.028 ± 0.005
Anaerobic	1 mM Fe^{2+}	0.074 ± 0.004	0.021 ± 0.005
Anaerobic	No Fe^{2+} added	0.066 ± 0.016	0.013 ± 0.005

[a]Production of the protein dihydrofolate reductase (DHFR) from its mRNA was used to monitor translational activity. Protein synthesis was assayed by measuring the rate of NADPH oxidation at Abs_{340} by DHFR. Average values are reported ± standard error of the mean (n=4). All ribosomes were normalized to 9 mg mL^{-1} before adding to translation reactions.

rProtein characterization. Ribosomes under all four growth conditions contained a full repertoire of rProteins, and were associated with additional proteins, as determined by mass spectrometry. These non-ribosomal proteins ranged in function from translation to central metabolism. Proteins from anaerobic pathways were generally more abundant in ribosomes from anaerobic cells while proteins from aerobic pathways were more abundant in ribosomes from aerobic cells (**Tables S1, S2**). Proteins for synthesis of enterobactin, an Fe^{3+}-binding siderophore, were more abundant in ribosomes from aerobic cells and from those grown without added Fe, while the bacterial non-heme ferritin subunit was more abundant in ribosomes from anaerobic cells regardless of the Fe^{2+} content in the media (**Table S2**). Several proteins were differentially expressed in pre-GOE ribosomes relative to other growth conditions (**Fig. 5**). Notably, pre-GOE ribosomes had five times the abundance of the protein YceD than ribosomes grown anaerobically without added Fe^{2+}. Pre-GOE ribosomes had one third the abundance of the rProtein S12 methylthiotransferase protein RimO and rRNA LSU methyltransferase K/L protein RlmL than ribosomes from aerobically grown cells with 1 mM Fe^{2+}.

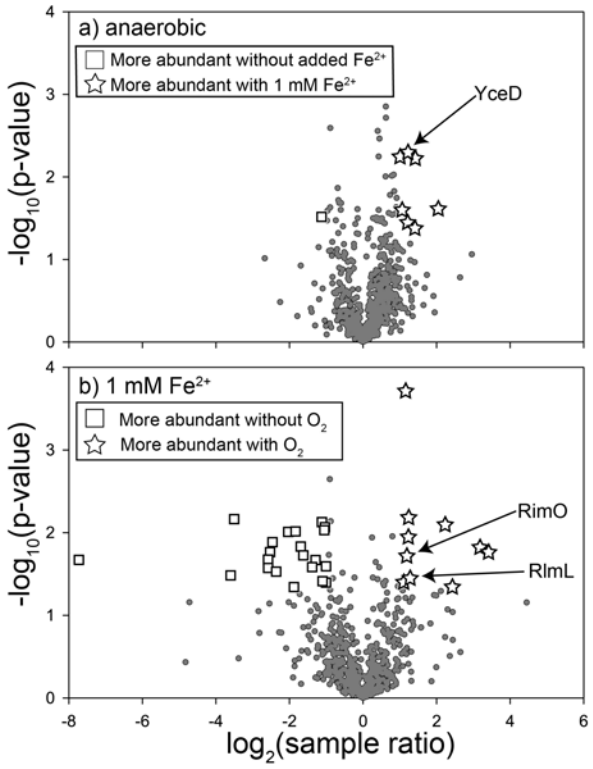

Figure 5. Differential protein abundance between ribosomes purified from cells grown under four growth conditions. Graphs display relative protein abundance in ribosome samples between two growth conditions. Black circles represent proteins not significantly more abundant in either sample. Gray rectangle and white stars represent proteins significantly more abundant in one of the samples. Proteins with a 2-fold or greater abundance in one sample versus another and a p-value less than or equal

435 to 0.05 (n=3), were classified as significantly more abundant.

436

437

438 **Discussion**

439 *Iron promotes rapid in-line cleavage of rRNA.* Mg^{2+} is known to cleave the RNA phosphodiester
440 backbone via an in-line mechanism (30,31). An oxidative cleavage mechanism for Mg^{2+}, with a
441 fixed oxidation state, is not accessible. We have shown here that Fe^{2+}, like Mg^{2+}, can cleave
442 RNA by a non-oxidative in-line mechanism. The apparent first-order rate constant for in-line
443 cleavage by Fe^{2+} is around 475-fold greater than for Mg^{2+}. We have used cleavage of 16S rRNA
444 to determine the apparent rate constants of both Mg^{2+}- and Fe^{2+}- mediated cleavage. For Mg^{2+},
445 the apparent rate constant, normalized for the number of phosphodiester bonds, is comparable to
446 previous reports (49), lending support to our results and highlighting the rapidity of cleavage by
447 Fe^{2+}. The in-line cleavage rate of Fe^{2+} relative to Mg^{2+} appears to place the rate constant of Fe^{2+}-
448 mediated cleavage above that of other metals that cause in-line cleavage, including Zn^{2+}, Pb^{2+},
449 Eu^{3+}, and Yb^{3+} (49).

450 Support for a non-oxidative in-line mechanism of cleavage of RNA by anoxic Fe^{2+} is provided
451 by observations that the rate of the reaction is not attenuated by anoxia and that the sites of
452 cleavage are conserved for Mg^{2+} and anoxic Fe^{2+}. The absence of hydroxyl radical intermediates
453 in the anoxic cleavage reaction is confirmed by the lack of inhibition by a radical quencher (25).
454 Direct Fe^{2+}-RNA interactions, as required for in-line cleavage (30,31) but not for Fenton
455 chemistry, are indicated by inhibition by the chelator EDTA. In-line cleavage is the dominant
456 mechanism of Fe^{2+} cleavage when contributions from Fenton-mediated processes are minimized
457 and is the only mechanism of Mg^{2+} cleavage, which is considerably slower. By contrast, in oxic
458 environments, transient Fe^{2+} oxidation generates hydroxyl radicals that cleave nucleic acids
459 (22,25-28).

460 Fe^{2+} appears to be a potent all-around cofactor for nucleic acids. The combined results indicate
461 that:

462 a) rRNA folds at lower concentration of Fe^{2+} than Mg^{2+} (23),
463 b) at least a subset of ribozymes and DNAzymes are more active in Fe^{2+} than in Mg^{2+}
464 (50,51),
465 c) the translation system is functional when Fe^{2+} is the dominant divalent cation (23),
466 d) at low concentrations of M^{2+}, T7 RNA polymerase is more active with Fe^{2+} than with
467 Mg^{2+} (52),
468 e) a broad variety of nucleic acid processing enzymes are active with Fe^{2+} instead of Mg^{2+}
469 (52),
470 f) rates of in-line cleavage are significantly greater for Fe^{2+} than for Mg^{2+} (here), and
471 g) Fe^{2+} but not Mg^{2+} confers oxidoreductase functionality to some RNAs (17,53).

472 *Why so fast?* Our previous DFT computations (52) help explain why Fe^{2+} is such a potent
473 cofactor for RNA. Conformations and geometries of coordination complexes with water and/or
474 phosphate are nearly identical for Fe^{2+} or Mg^{2+}. However, differences between Mg^{2+} and Fe^{2+} are
475 seen in the electronic structures of coordination complexes.

Firstly, because of low lying d orbitals, Fe^{2+} has greater electron withdrawing power than Mg^{2+} from first shell phosphate ligands. In coordination complexes with phosphate groups, the phosphorus atom is a better electrophile when $M^{2+} = Fe^{2+}$ than when $M^{2+} = Mg^{2+}$. This difference between Mg^{2+} and Fe^{2+} is apparent in ribozyme reactions and in-line cleavage reactions.

Secondly, $Fe^{2+}(H_2O)_6$ is a stronger acid than $Mg^{2+}(H_2O)_6$; depletion of electrons is greater from water molecules that coordinate Fe^{2+} than from those that coordinate Mg^{2+}. The lower pKa of $Fe^{2+}(H_2O)_6$ may promote protonation of the 5'OH leaving group during cleavage. Additionally, the superior electron-depleting power of Fe^{2+} may better promote activation of the 2'-OH nucleophile. Metal hydrates with low pKa's have been reported to induce RNA cleavage better than less acidic metal hydrates (30).

The mechanisms of in-line cleavage suggest that direct M^{2+}-RNA coordination is required (30,31). Indeed, studies of the in-line fragment patterns have previously been used to probe structural information on RNA molecules, such as determination of metal-binding sites (34,35).

Ribosomal iron content is elevated in vivo *by pre-GOE conditions*. Our data show for the first time that environmental conditions can affect the *in vivo* iron content of bacterial ribosomes. Ribosomal Fe content in cells is impacted by the availability and reactivity of Fe^{2+} and O_2. In oxic conditions, extracellular Fe is insoluble, and is difficult for cells to assimilate (54), requiring siderophores like enterobactin for Fe^{3+} uptake (55,56). Once in the cell, byproducts of aerobic metabolism, such as H_2O_2 and O_2^-, or O_2 can react with Fe^{2+} to form hydroxyl radicals (22,28,57). Thus, aerobic cells tightly regulate intracellular Fe to maintain low Fe^{2+} levels in the cytosol (58), minimizing Fe^{2+} availability for incorporation into ribosomes. We detect only around 1-2 Fe^{2+} per ribosome in aerobic growth conditions, consistent to what was previously seen for yeast ribosomes (59). In anoxic conditions, Fe^{2+} is more bioavailable and is less harmful because anaerobic growth generates fewer reactive oxygen species and there is no threat from O_2 diffusion into cells. Thus, anaerobic cells do not sequester Fe, and labile Fe^{2+} accumulates in the cytoplasm (55). Under pre-GOE conditions, Fe^{2+} is abundant and bioavailable, allowing cellular assimilation (60). We detect around 9 Fe^{2+} per ribosome in pre-GOE conditions.

Fe^{2+} associates with rRNA in vivo. Exchange of non-native metals for native metals is well-known during purification of proteins (61). We observe analogous phenomena with rRNA. Fe^{2+} can exchange with Mg^{2+} (and vice versa) during purification of ribosomes. Ribosomes purified in either Fe^{2+} or Mg^{2+} associate with 500-1000 M^{2+} ions that match the type of ion in the purification buffers.

However, our data support the tight association and lack of exchange of around 9 M^{2+} per ribosome. This subset of M^{2+} do not exchange during purification. The number of non-exchangeable M^{2+} closely matches the number of M^{2+} identified previously as a special class of deeply buried and highly coordinated M^{2+} in dinuclear microclusters (M^{2+}-μc's) (16). Mg^{2+} ions in M^{2+}-μc's are directly chelated by multiple phosphate oxygens of the rRNA backbone and are substantially dehydrated. M^{2+}-μc's within the LSU provide a framework for the ribosome's peptidyl transferase center, the site of protein synthesis in the ribosome, suggesting an essential and ancient role for M^{2+}-μc's in the ribosome. There are four dinuclear M^{2+}-μc's in the LSU and one in the SSU, accounting for 10 M^{2+} (16). Displacement of these M^{2+} would require large-scale changes in ribosomal conformation. In sum, there are ten M^{2+} per ribosome that are expected to

be refractory to exchange. We hypothesize that this subset M^{2+} are contained in M^{2+} -µc's, which can be occupied by either Mg^{2+} or Fe^{2+} (17), depending on growth conditions.

We also hypothesize that ribosomes harvested from aerobic cells have low Fe^{2+}/Mg^{2+} ratios because of low intracellular Fe^{2+} availability and lability. This hypothesis is supported by our observation that the number of slow exchanging Fe^{2+} per ribosome from aerobic cells is near the baseline of our measurements. It appears that ribosomes harvested from pre-GOE conditions have high Fe^{2+}/Mg^{2+} ratios because of high intracellular Fe^{2+} availability and lability, as indicated by the close match in the number of slowly exchanging Fe^{2+} per ribosome and the number of available M^{2+} sites in ribosomal M^{2+}-µc's. In these experiments we detect only the Fe^{2+} ions that do not exchange during purification.

Anoxic Fe^{2+} degrades rRNA within ribosomes. rRNA from all four growth conditions showed partial hydrolysis when ribosomes were purified in anoxic Fe^{2+}. It appears that Fe^{2+} can mediate rRNA degradation by an in-line mechanism during ribosomal purification in anoxic Fe^{2+}. Less rRNA cleavage was observed in ribosomes purified with Mg^{2+}, which contain orders of magnitude lower Fe^{2+}.

What about proteins? While eukaryotic iron binding rProteins have been reported (62), to our knowledge, there are currently no reports of prokaryotic iron binding rProteins. However, our MS analysis indicates a variety of non-rProteins co-purified with the ribosome and presumably associate with the ribosome *in vivo*. Some of these may represent nascent polypeptide being translated at the time of cell harvesting. Several of the ribosome-associated proteins are known to bind to iron. A notable example is the bacterial non-heme ferritin subunit protein, which is associated with the ribosome in each of our growth conditions. Bacterial non-heme ferritin is an iron storage protein that can hold as many as 3,000 Fe^{3+} atoms as the mineral ferrihydrite (56) in a 24-mer of identical subunits that self-assemble into the mature protein (63). There is previous evidence for ferritin copurifying with ribosomes in sucrose gradients. The use of column purification in our study makes coincidental copurification unlikely, and supports direct association of ferritin with ribosomes (64). Non-heme ferritin is upregulated under high intracellular iron so it is perhaps unsurprising that this protein is most abundant in ribosomes from pre-GOE conditions (65,66). We cannot discount the contribution of iron loaded ferritin towards the elevated ribosomal iron content. However, recent evidence suggests that ferritin-bound iron makes up a very small portion of the total iron pool in exponentially growing *E. coli* (67).

Differential expression of YceD under pre-GOE conditions. We used mass spectrometry to determine if pre-GOE growth conditions had any significant effect on the rProtein or ribosome-associated protein content of our samples. The only protein predicted to be involved in ribosome function or assembly that was significantly more abundant under pre-GOE conditions was the large rRNA subunit accumulation protein YceD. YceD is a 173 amino acid protein with a single C-$X_{(2)}$-C cysteine motif suggesting a potential metal binding site. The function of YceD remains unclear. The *yceD* gene is co-transcribed with the rProtein L32 gene *rpmF*. *ΔyceD* mutants had decreased 23S rRNA content compared to the wild type, suggesting that YceD is involved in 23S rRNA synthesis and/or processing (68). The higher abundance of YceD associated with pre-GOE ribosomes suggests that YceD may play a role in incorporating Fe^{2+} into the ribosome *in vivo*. Proteins that were less abundant in pre-GOE ribosomes included rProtein S12 methylthiotransferase protein RimO and the rRNA LSU methyltransferase K/L. While the

functions of these protein and rRNA modifications in the ribosome are not totally clear, some evidence points to structural roles (67). Whatever their utility, their reduced abundance in pre-GOE ribosomes suggests that the increased Fe^{2+} association in these ribosomes may render the function of these proteins less important.

Cellular significance of the newfound Fe^{2+}-RNA and ribosome relationship. Given the presence of M^{2+}-µc's in the universal common core of ribosomes (17), and our finding that Fe^{2+} may occupy M^{2+}-µc's *in vivo*, a diversity of ribosomes, including those of humans, may specifically incorporate Fe^{2+}. Iron in the ribosome correlates with a modified abundance of select rProteins, possibly causing altered translation and gene expression. Moreover, iron likely decreases ribosome longevity within the cell, as we have illustrated the potency of Fe^{2+} in inducing rRNA cleavage. In fact, rRNA cleavage events commonly linked to Fe^{2+} oxidation, such as in the human ribosome factoring in Alzheimer's disease (69), or in *Saccharomyces cerevisiae* rRNA where cleavage is tied to downstream oxidative stress response (59) could be in some measure attributable to Fe^{2+} in-line cleavage. The rapid Fe^{2+} in-line cleavage phenomena can be expected to hold to any RNAs regardless of the presence of an oxidant, given they do not specifically coordinate or shield themselves from the iron to prevent cleavage. We have uncovered a new avenue for RNA to act as a response molecule in Fe regulation or stress pathways and highlighted a potential mechanism by which Fe^{2+} induces cellular toxicity particularly relevant to anoxic environments. Involvement of Fe^{2+} in RNA offers fine-tuning within cellular systems, in that in one capacity it is a cofactor and in another it causes in-line cleavage.

Summary. Here we have shown for the first time that bacteria grown in pre-GOE conditions contain functional ribosomes with tightly bound Fe atoms. The ~10 ribosomal Fe ions in pre-GOE ribosomes are likely deeply buried and specifically bound to rRNA. Depending on intracellular Fe lability, ribosomes may have higher Fe content *in vivo* given the high capacity for the ribosome to substitute ~600 loosely bound Mg^{2+} ions for Fe^{2+}. Furthermore, direct association of the naked rRNA with Fe atoms results in a fast rate of in-line cleavage. This highlights a potential role of protection from in-line cleavage for rProteins, and also suggests that iron may drive ribosomes through a rapid life cycle. Our results support a model in which alternate M^{2+} ions, namely Fe^{2+}, participated in the origin and early evolution of life: first in abiotic proto-biochemical systems, through potentially rapid rounds of formation and breakdown of RNA structures, and then within early cellular life up until the GOE (70). Our study also expands the role of Fe^{2+} in modern biochemistry by showing that extant life retains the ability to incorporate Fe into ribosomes. We surmise that extant organisms under certain environmental and cellular states may use Fe^{2+} as a ribosomal cofactor. In addition, obligate anaerobic organisms that have spent the entirety of their evolutionary history in permanently anoxic environments may still use abundant Fe^{2+} in their ribosomes *in vivo*.

Funding. This work was supported by the National Aeronautics and Space Administration Astrobiology program grants NNX14AJ87G, NNX16AJ28G, NNX16AJ29G, and 80NSSC18K1139 under the Center for Origin of Life. The TXRF was supported by National Institutes of Health Grant ES025661 (to A. R. R.) and National Science Foundation Grant MCB-1552791 (to A. R. R.).

Acknowledgments. We thank Corinna Tuckey (New England BioLabs), Eric B. O'Neill, and Drs. Anton Petrov, Roger M. Wartell, Thomas Tullius, and Ada Yonath for helpful discussions.

606

References

1. Bernier, C.R., Petrov, A.S., Kovacs, N.A., Penev, P.I. and Williams, L.D. (2018) Translation: The Universal Structural Core of Life. *Mol. Biol. Evol.*, **35**, 2065-2076.

2. Melnikov, S., Ben-Shem, A., Garreau de Loubresse, N., Jenner, L., Yusupova, G. and Yusupov, M. (2012) One core, two shells: bacterial and eukaryotic ribosomes. *Nat. Struct. Mol. Biol.*, **19**, 560-567.

3. Woese, C.R. (2001) Translation: in retrospect and prospect. *RNA*, **7**, 1055-1067.

4. Noller, H.F., Kop, J., Wheaton, V., Brosius, J., Gutell, R.R., Kopylov, A.M., Dohme, F., Herr, W., Stahl, D.A. and Gupta, R. (1981) Secondary structure model for 23S ribosomal RNA. *Nucleic Acids Res.*, **9**, 6167-6189.

5. Petrov, A.S., Bernier, C.R., Hsiao, C., Norris, A.M., Kovacs, N.A., Waterbury, C.C., Stepanov, V.G., Harvey, S.C., Fox, G.E., Wartell, R.M. *et al.* (2014) Evolution of the ribosome at atomic resolution. *Proc. Natl. Acad. Sci. USA*, **111**, 10251-10256.

6. Bokov, K. and Steinberg, S.V. (2009) A hierarchical model for evolution of 23S ribosomal RNA. *Nature*, **457**, 977-980.

7. Kovacs, N.A., Petrov, A.S., Lanier, K.A. and Williams, L.D. (2017) Frozen in Time: The History of Proteins. *Mol. Biol. Evol.*, **34**, 1252-1260.

8. Agmon, I., Bashan, A. and Yonath, A. (2006) On ribosome conservation and evolution. *Isr. J. Ecol. Evol.*, **52**, 359-374.

9. Klein, D.J., Moore, P.B. and Steitz, T.A. (2004) The contribution of metal ions to the structural stability of the large ribosomal subunit. *RNA*, **10**, 1366-1379.

10. Anbar, A.D. (2008) Elements and evolution. *Science*, **322**, 1481-1483.

11. Hazen, R.M. and Ferry, J.M. (2010) Mineral evolution: Mineralogy in the fourth dimension. *Elements*, **6**, 9-12.

12. Holland, H.D. (2006) The oxygenation of the atmosphere and oceans. *Philos. Trans. R. Soc. London, Ser. B*, **361**, 903-915.

13. Klein, C. (2005) Some Precambrian banded iron-formations (BIFs) from around the world: Their age, geologic setting, mineralogy, metamorphism, geochemistry, and origins. *Am. Mineral.*, **90**, 1473-1499.

14. Holland, H.D. (1973) The oceans; a possible source of iron in iron-formations. *Econ. Geol.*, **68**, 1169-1172.

15. Bowman, J.C., Lenz, T.K., Hud, N.V. and Williams, L.D. (2012) Cations in charge: magnesium ions in RNA folding and catalysis. *Curr Opin Struct Biol*, **22**, 262-272.

16. Hsiao, C. and Williams, L.D. (2009) A recurrent magnesium-binding motif provides a framework for the ribosomal peptidyl transferase center. *Nucleic Acids Res.*, **37**, 3134-3142.

17. Lin, S.Y., Wang, Y.C. and Hsiao, C. (2019) Prebiotic Iron Originates the Peptidyl Transfer Origin. *Mol. Biol. Evol.*, **36**, 999-1007.

18. Schuwirth, B.S., Borovinskaya, M.A., Hau, C.W., Zhang, W., Vila-Sanjurjo, A., Holton, J.M. and Cate, J.H.D. (2005) Structures of the Bacterial Ribosome at 3.5 Å Resolution. *Science*, **310**, 827-834.

19. Selmer, M., Dunham, C.M., Murphy, F.V., Weixlbaumer, A., Petry, S., Kelley, A.C., Weir, J.R. and Ramakrishnan, V. (2006) Structure of the 70S ribosome complexed with mRNA and tRNA. *Science*, **313**, 1935-1942.

20. Demeshkina, N., Jenner, L., Westhof, E., Yusupov, M. and Yusupova, G. (2012) A new understanding of the decoding principle on the ribosome. *Nature*, **484**, 256-259.

21. Petrov, A.S., Bernier, C.R., Hsiao, C., Okafor, C.D., Tannenbaum, E., Stern, J., Gaucher, E., Schneider, D., Hud, N.V., Harvey, S.C. *et al.* (2012) RNA-magnesium-protein interactions in large ribosomal subunit. *J. Phys. Chem. B*, **116**, 8113-8120.

22. Winterbourn, C.C. (1995) Toxicity of iron and hydrogen peroxide: the Fenton reaction. *Toxicol. Lett.*, **82**, 969-974.

23. Bray, M.S., Lenz, T.K., Haynes, J.W., Bowman, J.C., Petrov, A.S., Reddi, A.R., Hud, N.V., Williams, L.D. and Glass, J.B. (2018) Multiple prebiotic metals mediate translation. *Proc. Natl. Acad. Sci. USA*, **115**, 12164-12169.

24. Lenz, T.K., Norris, A.M., Hud, N.V. and Williams, L.D. (2017) Protein-free ribosomal RNA folds to a near-native state in the presence of Mg^{2+}. *RSC Advances*, **7**, 54674-54681.

25. Dixon, W.J., Hayes, J.J., Levin, J.R., Weidner, M.F., Dombroski, B.A. and Tullius, T.D. (1991) Hydroxyl radical footprinting. *Methods Enzymol.*, **208**, 380-413.

26. Tullius, T.D. (1996) In Suslick, K. (ed.), *Comprehensive Supramolecular Chemistry*. Elsevier, Tarrytown, NY, Vol. 5, pp. 317-343.

27. Celander, D.W. and Cech, T.R. (1991) Visualizing the higher order folding of a catalytic RNA molecule. *Science*, **251**, 401-407.

28. Li, Z., Wu, J. and Deleo, C.J. (2006) RNA damage and surveillance under oxidative stress. *IUBMB Life*, **58**, 581-588.

29. Shcherbik, N. and Pestov, D.G. (2019) The Impact of Oxidative Stress on Ribosomes: From Injury to Regulation. *Cells*, **8**, 1379.

30. Forconi, M. and Herschlag, D. (2009) Metal ion-based RNA cleavage as a structural probe. *Methods Enzymol.*, **468**, 91-106.

31. Soukup, G.A. and Breaker, R.R. (1999) Relationship between internucleotide linkage geometry and the stability of RNA. *RNA*, **5**, 1308-1325.

32. Winkler, W., Nahvi, A. and Breaker, R.R. (2002) Thiamine derivatives bind messenger RNAs directly to regulate bacterial gene expression. *Nature*, **419**, 952-956.

679 33. Winkler, W.C., Nahvi, A., Roth, A., Collins, J.A. and Breaker, R.R. (2004) Control of gene
680 expression by a natural metabolite-responsive ribozyme. *Nature*, **428**, 281.

681 34. Dorner, S. and Barta, A. (1999) Probing ribosome structure by europium-induced RNA cleavage.
682 *Biol. Chem.*, **380**, 243-251.

683 35. Winter, D., Polacek, N., Halama, I., Streicher, B. and Barta, A. (1997) Lead-catalysed specific
684 cleavage of ribosomal RNAs. *Nucleic Acids Res.*, **25**, 1817-1824.

685 36. Pyle, A.M. (2002) Metal ions in the structure and function of RNA. *J. Biol. Inorg. Chem.*, **7**, 679-
686 690.

687 37. Pan, T. and Uhlenbeck, O.C. (1992) In vitro selection of RNAs that undergo autolytic cleavage
688 with lead (2+). *Biochemistry*, **31**, 3887-3895.

689 38. Riemer, J., Hoepken, H.H., Czerwinska, H., Robinson, S.R. and Dringen, R. (2004) Colorimetric
690 ferrozine-based assay for the quantitation of iron in cultured cells. *Anal. Biochem.*, **331**, 370-375.

691 39. Maguire, B.A., Wondrack, L.M., Contillo, L.G. and Xu, Z. (2008) A novel chromatography
692 system to isolate active ribosomes from pathogenic bacteria. *RNA*, **14**, 188-195.

693 40. Shimizu, Y., Inoue, A., Tomari, Y., Suzuki, T., Yokogawa, T., Nishikawa, K. and Ueda, T.
694 (2001) Cell-free translation reconstituted with purified components. *Nature Biotechnol.*, **19**, 751-
695 755.

696 41. Connors, K. (1990) *Chemical Kinetics: The Study of Reaction Rates in Solution*. VCH Publishers,
697 Inc., New York, NYd.

698 42. Hsiao, C., Lenz, T.K., Peters, J.K., Fang, P.-Y., Schneider, D.M., Anderson, E.J., Preeprem, T.,
699 Bowman, J.C., O'Neill, E.B. and Lie, L. (2013) Molecular paleontology: a biochemical model of
700 the ancestral ribosome. *Nucleic Acids Res.*, **41**, 3373-3385.

701 43. Rappsilber, J., Mann, M. and Ishihama, Y. (2007) Protocol for micro-purification, enrichment,
702 pre-fractionation and storage of peptides for proteomics using StageTips. *Nat Protoc*, **2**, 1896-
703 1906.

704 44. Cox, J. and Mann, M. (2008) MaxQuant enables high peptide identification rates, individualized
705 p.p.b.-range mass accuracies and proteome-wide protein quantification. *Nat. Biotechnol.*, **26**,
706 1367-1372.

707 45. Cox, J., Neuhauser, N., Michalski, A., Scheltema, R.A., Olsen, J.V. and Mann, M. (2011)
708 Andromeda: a peptide search engine integrated into the MaxQuant environment. *J Proteome Res*,
709 **10**, 1794-1805.

710 46. Kurylo, C.M., Alexander, N., Dass, R.A., Parks, M.M., Altman, R.A., Vincent, C.T., Mason, C.E.
711 and Blanchard, S.C. (2016) Genome Sequence and Analysis of *Escherichia coli* MRE600, a
712 Colicinogenic, Nonmotile Strain that Lacks RNase I and the Type I Methyltransferase, EcoKI.
713 *Genome Biol Evol*, **8**, 742-752.

47. Tyanova, S., Temu, T., Sinitcyn, P., Carlson, A., Hein, M.Y., Geiger, T., Mann, M. and Cox, J. (2016) The Perseus computational platform for comprehensive analysis of (prote)omics data. *Nat. Methods*, **13**, 731-740.

48. Tullius, T.D., Dombroski, B.A., Churchill, M.E. and Kam, L. (1987) Hydroxyl radical footprinting: A high-resolution method for mapping protein-DNA contacts. *Methods Enzymol.*, **155**, 537-558.

49. Breslow, R. and Huang, D.-L. (1991) Effects of metal ions, including Mg^{2+} and lanthanides, on the cleavage of ribonucleotides and RNA model compounds. *Proc. Natl. Acad. Sci. USA*, **88**, 4080-4083.

50. Athavale, S.S., Petrov, A.S., Hsiao, C., Watkins, D., Prickett, C.D., Gossett, J.J., Lie, L., Bowman, J.C., O'Neill, E. and Bernier, C.R. (2012) RNA folding and catalysis mediated by iron (II). *PLoS One*, **7**, e38024.

51. Moon, W.J. and Liu, J. (2019) Replacing Mg(2+) by Fe(2+) for RNA-Cleaving DNAzymes. *ChemBioChem*, https://doi.org/10.1002/cbic.201900344.

52. Okafor, C.D., Lanier, K.A., Petrov, A.S., Athavale, S.S., Bowman, J.C., Hud, N.V. and Williams, L.D. (2017) Iron mediates catalysis of nucleic acid processing enzymes: Support for Fe(II) as a cofactor before the Great Oxidation Event. *Nucleic Acids Res.*, **45**, 3634-3642.

53. Hsiao, C., Chou, I.-C., Okafor, C.D., Bowman, J.C., O'neill, E.B., Athavale, S.S., Petrov, A.S., Hud, N.V., Wartell, R.M., Harvey, S.C. *et al.* (2013) RNA with iron (II) as a cofactor catalyses electron transfer. *Nat. Chem.*, **5**, 525-528.

54. Morgan, B. and Lahav, O. (2007) The effect of pH on the kinetics of spontaneous Fe(II) oxidation by O2 in aqueous solution--basic principles and a simple heuristic description. *Chemosphere*, **68**, 2080-2084.

55. Beauchene, N.A., Mettert, E.L., Moore, L.J., Keleş, S., Willey, E.R. and Kiley, P.J. (2017) O2 availability impacts iron homeostasis in *Escherichia coli*. *Proc. Natl. Acad. Sci. USA*, **114**, 12261-12266.

56. Andrews, S., Norton, I., Salunkhe, A.S., Goodluck, H., Aly, W.S.M., Mourad-Agha, H. and Cornelis, P. (2013) In Banci, L. (ed.), *Metallomics and the Cell*. Springer Netherlands, pp. 203-239.

57. Keyer, K. and Imlay, J.A. (1996) Superoxide accelerates DNA damage by elevating free-iron levels. *Proc. Natl. Acad. Sci. USA*, **93**, 13635-13640.

58. Braun, V. and Hantke, K. (2011) Recent insights into iron import by bacteria. *Current Opin. Chem. Biol.*, **15**, 328-334.

59. Zinskie, J.A., Ghosh, A., Trainor, B.M., Shedlovskiy, D., Pestov, D.G. and Shcherbik, N. (2018) Iron-dependent cleavage of ribosomal RNA during oxidative stress in the yeast *Saccharomyces cerevisiae*. *J Biol Chem*, **293**, 14237-14248.

60. Hohle, T.H. and O'brian, M.R. (2016) Metal□specific control of gene expression mediated by *Bradyrhizobium japonicum* Mur and *Escherichia coli* Fur is determined by the cellular context. *Molecular Microbiology*, **101**, 152-166.

61. Handing, K.B., Niedzialkowska, E., Shabalin, I.G., Kuhn, M.L., Zheng, H. and Minor, W. (2018) Characterizing metal-binding sites in proteins with X-ray crystallography. *Nat. Protoc.*, **13**, 1062.

62. Furukawa, T., Uchiumi, T., Tokunaga, R. and Taketani, S. (1992) Ribosomal protein P2, a novel iron-binding protein. *Archives of Biochemistry and Biophysics*, **298**, 182-186.

63. Zhang, Y. and Orner, B.P. (2011) Self-assembly in the ferritin nano-cage protein superfamily. *Int J Mol Sci*, **12**, 5406-5421.

64. Helgeland, L. (1968) The ferritin content of the free ribosome fraction isolated from adult male and female rat liver. *FEBS Lett.*, **1**, 308-310.

65. Massé, E. and Arguin, M. (2005) Ironing out the problem: new mechanisms of iron homeostasis. *Trends in Biochemical Sciences*, **30**, 462-468.

66. Nandal, A., Huggins, C.C., Woodhall, M.R., McHugh, J., Rodriguez-Quinones, F., Quail, M.A., Guest, J.R. and Andrews, S.C. (2010) Induction of the ferritin gene (ftnA) of *Escherichia col*i by Fe(2+)-Fur is mediated by reversal of H-NS silencing and is RyhB independent. *Mol. Microbiol.*, **75**, 637-657.

67. Wofford, J.D., Bolaji, N., Dziuba, N., Outten, F.W. and Lindahl, P.A. (2019) Evidence that a respiratory shield in *Escherichia coli* protects a low-molecular-mass FeII pool from O2-dependent oxidation. *J. Biol. Chem.*, **294**, 50-62.

68. Yang, J., Suzuki, M. and McCarty, D.R. (2016) Essential role of conserved DUF177A protein in plastid 23S rRNA accumulation and plant embryogenesis. *J. Exp. Bot.*, **67**, 5447-5460.

69. Honda, K., Smith, M.A., Zhu, X., Baus, D., Merrick, W.C., Tartakoff, A.M., Hattier, T., Harris, P.L., Siedlak, S.L., Fujioka, H. *et al.* (2005) Ribosomal RNA in Alzheimer disease is oxidized by bound redox-active iron. *J Biol Chem*, **280**, 20978-20986.

70. Okafor, C.D., Bowman, J.C., Hud, N.V., Glass, J.B. and Williams, L.D. (2018), *Prebiotic Chemistry and Chemical Evolution of Nucleic Acids*. Springer, pp. 227-243.